

20 Abstract

21 We illustrate offsets in surface seawater isotopic composition between recent, public
22 data sets from the Atlantic Ocean and the subtropical South-East Indian Ocean. The
23 observed offsets between data sets often exceed 0.10‰ in $\delta^{18}\text{O}$ and 0.50‰ in $\delta^2\text{H}$. They
24 might in part originate from different sampling of seasonal, interannual or spatial
25 variability. However, they likely mostly originate from different instrumentations and
26 protocols used to measure the water samples. Estimation of the systematic offsets is
27 required before merging the different data sets in order to investigate spatio-temporal
28 variability of isotopic composition in the world ocean surface waters. This highlights the
29 need to actively share seawater isotopic composition samples dedicated to specific
30 intercomparison of data produced in the different laboratories.

31

32

33 1. Introduction

34 Seawater isotopic composition ($^{18}\text{O}/^{16}\text{O}$ and $^2\text{H}/^1\text{H}$ ratios expressed as $\delta^{18}\text{O}$ and $\delta^2\text{H}$ in
35 ‰ in the VSMOW/SLAP scale) is classified as an Essential Ocean/Climate Variable
36 (EOV/ECV) in international programs such as GEOTRACES and GO-SHIP. Stable
37 seawater isotopes ($\delta^{18}\text{O}$, $\delta^2\text{H}$) are used to trace sources of freshwater (precipitation,
38 evaporation, runoff, melting glaciers, sea ice formation and melting), both at the ocean
39 surface and in the ocean interior (Schmidt et al., 2007; Hilaire-Marcel et al., 2021).
40 Except for fractionation during phase changes, the water isotopic composition is nearly
41 conservative in the ocean.

42 A major emphasis is on high latitude oceanography. There, continental (or iceberg)
43 glacial melt, formation or melt of sea ice, and high-latitude river inputs (for the Arctic)
44 leave imprints on the surface ocean isotopic composition, as well as below the surface
45 down to 800 m close to ice shelves in the southern ocean (Randall-Goodwin et al., 2015;
46 Biddle et al., 2019, Hennig et al., 2024). In contrast, few studies have been performed on
47 the isotopic signature in the deep ocean (e.g., Prasanna et al., 2015; Voelker et al., 2015).
48 Seawater isotopes in the upper ocean at low latitudes are often vital for paleoclimatic
49 studies, as they are needed to calibrate proxies of past ocean variability in marine
50 carbonate records such as corals and foraminifera (e.g., PAGES CoralHydro2k working
51 group; Konecky et al., 2020). Seawater isotopes are also important tracers in the coastal
52 ocean, with emphasis on upwelling (Conroy et al., 2014, 2017; Kubota et al., 2022; Lao et
53 al., 2022), and river discharges (e.g., Amazon) (Karr and Showers, 2001). Surface ocean
54 seawater isotopes are also used to characterize evaporation rates and air-sea
55 interactions (Benetti et al., 2017).

56 The isotopic signatures of these different processes are evolving in our warming world,
57 which will imprint on the seawater isotopic composition (Oppo et al., 2007).

58 Additionally, seawater isotope data provide model boundary conditions and allow the
59 assessment of model performance in isotope-enabled Earth system models (e.g. Schmidt
60 et al., 2007; Brady et al., 2019; Cauquoin et al., 2019), thereby improving climate model
61 projections of the future.

62 Stable seawater isotope data have thus been massively produced in the last decades by
63 a variety of methods. For example, most data compiled in the “GISS Global Seawater
64 Oxygen-18 Database -V1.21” for stable seawater isotopes (LeGrande and Schmidt, 2006)
65 originate from Isotope-ratio Mass Spectrometry (IRMS). They were mostly measured in
66 earlier decades by dual-inlet technology (highest precision), whereas, more recently, the
67 continuous-flow method (lower precision) became widespread for seawater isotope
68 analysis. In the last decade, cavity ring-down spectroscopy (CRDS) turned into another
69 commonly used method as it allows parallel measurement of $\delta^{18}\text{O}$ and $\delta^2\text{H}$, but with
70 often lower precision, at least early on (e.g., Voelker et al., 2015).

71 Reverdin et al. (2022) recently compiled a mix of data produced by IRMS and CRDS at
72 LOCEAN (<https://www.seanoe.org/data/00600/71186/>). As CRDS and other laser
73 techniques (Glaubke et al., 2024) have become more prevalent recently, they contribute
74 a significant part of the new data produced and thus also to the soon to be released
75 CoralHydro2k seawater database for $\delta^{18}\text{O}$ ($\delta^2\text{H}$) (focus on the tropics (35°N - 35°S);
76 Atwood et al., 2024).

77 There are potential differences between the data produced by the two methods.
78 Typically, CO_2 -water or H_2 -water equilibration was used for the IRMS measurements
79 and yields measurements of the activity of water, which decreases with increasing
80 salinity. Furthermore, concentration of divalent cations like Mg^{++} are responsible
81 for slight changes in fractionation factors. On the other hand, the laser methods such as
82 CRDS evaporate the entire sample. If the samples have not been distilled beforehand,
83 there is an issue of salt deposition and of resulting absorption or desorption of water
84 with fractionation effects. In the LOCEAN database (Reverdin et al., 2022), an attempt
85 was made to adjust the data, based on the analysis of Benetti et al (2017b). This was also
86 adopted by at least one other group (Haumann et al., 2022), but overall, there is the
87 possibility of an offset of these data with respect to the ones of other groups using CRDS.
88 However, it should be noted that some studies reporting unadjusted $\delta^{18}\text{O}$ measurements
89 from CRDS and IRMS technique with CO_2 -water equilibration provide data that were
90 undistinguishable within instrumental precision (Walker et al., 2016; Hennig et al.,
91 2024).

92 It is actually quite common when using water isotope data in studies involving more
93 than one data set, to first evaluate whether there are possible offsets. Intercomparison
94 with earlier data or reference materials was a prerequisite for GEOTRACES sampling
95 campaigns, although for the water isotopes this was, unfortunately, seldomly followed
96 (e.g., Voelker et al., 2015). These intercomparisons often outline systematic differences
97 which could result from the issue outlined above, or from other issues, such as
98 uncertainties in reference materials used, analysis protocols, or isotopic changes in the
99 samples during their handling and storage (Benetti et al., 2017a; Akhoudas et al., 2019;
100 Hennig et al., 2024). In other cases, this was not done, either because the data stood by
101 themselves (Bonne et al., 2019, for $\delta^{18}\text{O}$ and $\delta^2\text{H}$ data), or there was no comparison data
102 available in the same region (Glaubke et al., 2024, for $\delta^{18}\text{O}$ data). The possible offsets can
103 however become an issue, when these data are placed in a larger context. For example,
104 Glaubke et al. (2024) identify a large difference in the S - $\delta^{18}\text{O}$ relationship in the
105 subtropical Indian Ocean between their data in the south-eastern part and other data in
106 the south-western Indian Ocean. They also discuss and question differences in the deep
107 water-masses isotopic values between separate data sets, but as these might also be
108 explained by large uncertainties in these data, we will not address them further.

109 Using these two examples (Bonne et al., 2019; Glaubke et al., 2024), the aim of this note
110 is to point out the interest when producing a new data set, of exchanging collected
111 samples to carry a direct comparison, or, if this was not done, to compare the data with
112 other published data and evaluate potential systematic differences.

113 2. Comparisons

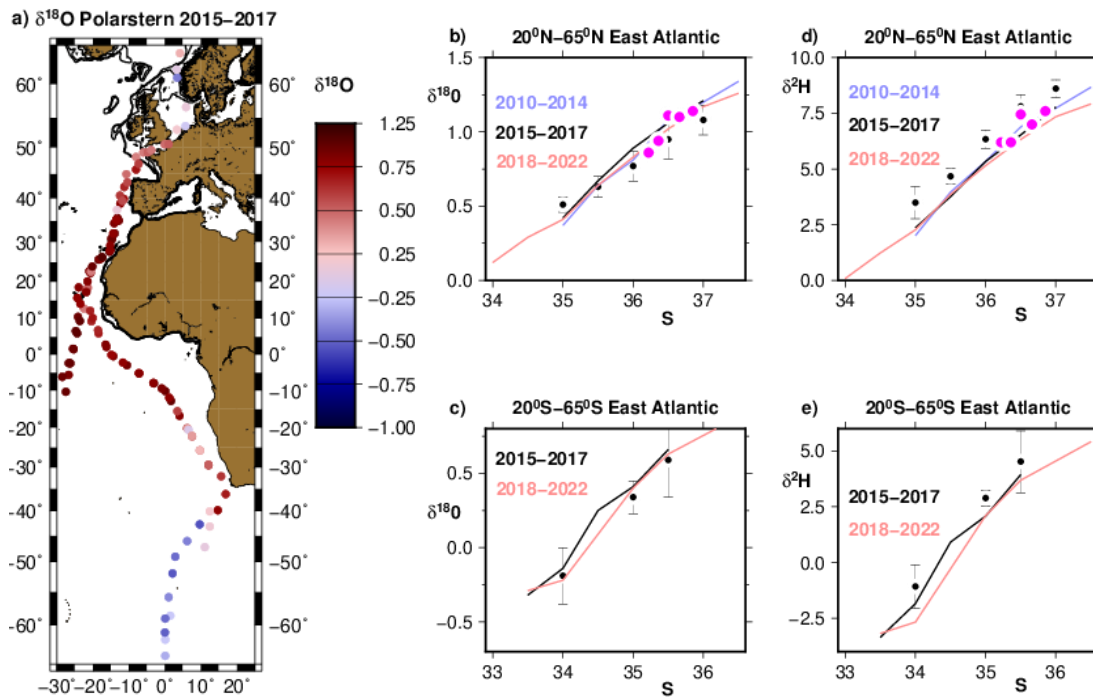
114 For identifying possible offsets, we consider surface ocean subsets of the LOCEAN data
115 base in specific regions for roughly the same years as the other data collected. The data
116 extracted are from the same regions as in the datasets of the two studies and are
117 gathered in S - $\delta^{18}\text{O}$ space as well as in S - $\delta^2\text{H}$ space (available only for the Bonne et al
118 (2019) data set), where S is reported as a practical salinity with the practical salinity
119 scale of 1978 (pss). The assumption done here as in many papers is that the S - $\delta^{18}\text{O}$
120 relationship holds on fairly large scales in the surface layer (for the eastern subtropical
121 North Atlantic, see for example, the discussion in Voelker et al (2015) and in Benetti et
122 al. (2017a)). Obviously, this has limitations, such as in areas influenced by more than

123 one water mass or by multiple freshwater end-members (meteoric, continental run-off,
124 sea ice melt or formation, evaporation).

125 2.1 Daily surface data collected from R.V. Polarstern

126 The surface seawater samples originated from daily collection during two years on
127 board RV Polarstern in 2015-2017 (Bonne et al., 2019). There is no salinity provided
128 with the data, and here we chose to associate them with the simultaneously collected
129 thermosalinograph (TSG) data collected on board the RV Polarstern and available from
130 PANGAEA (for each cruise, an indexed file with title starting by 'Continuous
131 thermosalinograph oceanography along Polarstern' is included in PANGAEA: for example,
132 TSG data for the first cruise (PS90) associated with the isotopic seawater data are found
133 at <https://doi.org/10.1594/PANGAEA.858885>). The water samples were not collected
134 from the same water line and pumping depth as the TSG data, which can result in
135 differences. This is however likely to be small in most circumstances away from large
136 freshwater input at the sea surface, such as from melting sea ice, intense rainfall and
137 river estuaries (Boutin et al., 2016). We also applied an adjustment of +0.25‰ to the
138 $\delta^{18}\text{O}$ data of Bonne et al. (2019), based on post-analysis identification of a bias in an
139 internal reference material.

140 We then estimate averages of all the data as a function of salinity in two domains
141 extending poleward of the subtropical salinity maximum toward the higher latitudes in
142 the eastern part of the Atlantic Ocean (thus, 20°N to 65°N and the same in the southern
143 hemisphere). This is done by sorting out the data by salinity classes of 0.5. The LOCEAN
144 data until 2016 in the North and tropical Atlantic were presented in Benetti et al
145 (2017a), showing the tightness of the S- $\delta^{18}\text{O}$ and S- $\delta^2\text{H}$ relationships in vast domains of
146 the eastern Atlantic. In the North Atlantic, LOCEAN data have been continuously
147 collected since 2011, and south of 10°S in the eastern Atlantic mostly since 2017.



148

149

150

151 Figure 1: Comparison to Bonne et al. (2019). (a) map of RV Polarstern original data set
 152 points in eastern Atlantic Ocean east of 30°W. Water isotopes-S scatter diagrams
 153 averaged as a function of salinity in 0.5 practical salinity bins (left for $\delta^{18}\text{O}$, and right for
 154 $\delta^2\text{H}$), top for the northern hemisphere and bottom for the southern hemisphere, east of
 155 30°W and outside of [20°N, 20°S]. The colored curves represent average relationships of
 156 water isotopes in the LOCEAN data base as a function of practical salinity for three
 157 different period ranges, whereas the black dots with error bars are the binned averages
 158 of the Bonne et al. (2019) RV Polarstern data in 2015-2017 (after adjustment of
 159 +0.25‰ to $\delta^{18}\text{O}$), with the root mean square of the variance reported as error bars. Five
 160 individual surface points from Voelker et al (2023) are also plotted (magenta dots).

161 The average relationships found in the LOCEAN data set for three periods overlay well
 162 in particular in the northern hemisphere. Uncertainties on individual curves (not
 163 shown) are estimated based on the scatter of individual data in each salinity bin. They
 164 are typically on the order of 0.01-0.02 (0.05-0.10) ‰ for $\delta^{18}\text{O}$ ($\delta^2\text{H}$) respectively in the
 165 northern hemisphere (top panel), and a little larger for the less sampled southern

166 hemisphere curves in 2015-2017. Sampling is usually also insufficient at the low end of
167 the salinity range, to reliably estimate an uncertainty. Thus, these different curves nearly
168 overlay within the sampling uncertainty. Five surface samples that were collected in the
169 Northeast Atlantic during the same years within the same salinity range (Voelker et al.,
170 2023), also fit well on the North Atlantic curves. The adjusted $\delta^{18}\text{O}$ data from Bonne et
171 al. (2019) are slightly shifted downward with respect to the curves (Fig. 1b, c), with the
172 plotted standard deviation of individual data around the average not overlapping the
173 LOCEAN data average curves in most cases for the same years 2015-2017. The situation
174 is opposite for the 35 salinity bin in the northern hemisphere, with the adjusted $\delta^{18}\text{O}$
175 data from Bonne et al. (2019) being above the three LOCEAN average curves, which
176 might be due to samples collected uniquely in the English Channel and North Sea by RV
177 Polarstern in this salinity range, whereas sampling is more geographically-spread in the
178 LOCEAN data base.

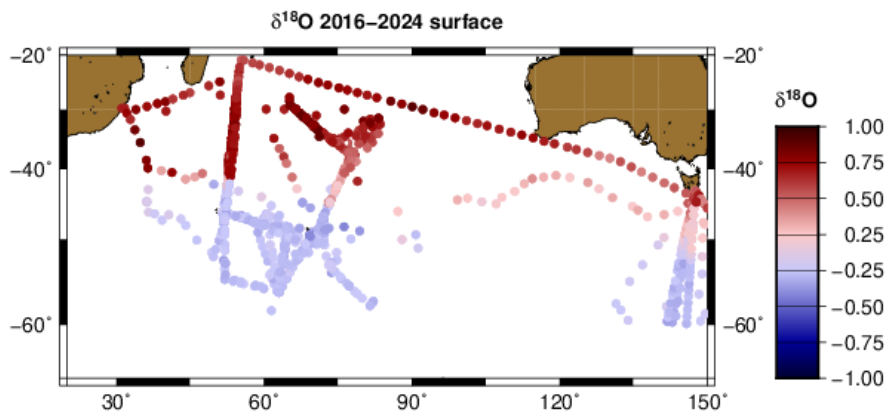
179 Altogether, the average $\delta^{18}\text{O}$ offset is small, with the LOCEAN data being higher by $0.02 \pm$
180 0.01 ‰ than the $\delta^{18}\text{O}$ from Bonne et al. (2019), which is not significantly different from
181 0 based on the interannual differences witnessed in the LOCEAN curves and the
182 scatter/uncertainty in the Polarstern data. A systematic difference is, however, found for
183 $\delta^2\text{H}$, with LOCEAN data been lower than $\delta^2\text{H}$ from Bonne et al. (2019) by $0.99 \pm 0.07 \text{ ‰}$
184 (Fig. 1d, e).

185

186 2.2 Southern subtropical Indian Ocean

187 Glaubke et al. (2024) describe a synthesis of water isotope data in the southern Indian
188 Ocean combining their new dataset in the southeastern Indian Ocean (CROCCA-2S) with
189 earlier data in the south-western Indian Ocean, in particular from LOCEAN, as well as
190 data from the south Australian shelf collected mostly in 2010 (Richardson et al., 2019),
191 and in the equatorial Indian Ocean (Kim et al., 2021). In the most recent version of the
192 LOCEAN data set, in addition to data included in Glaubke et al. (2024) for comparison
193 and collected mostly west of 80°E , there are two transects with surface data through the
194 southeastern Indian Ocean, one collected in February 2017, and the other in March
195 2024, thus in mid to late austral summer. These transects cross the region covered by

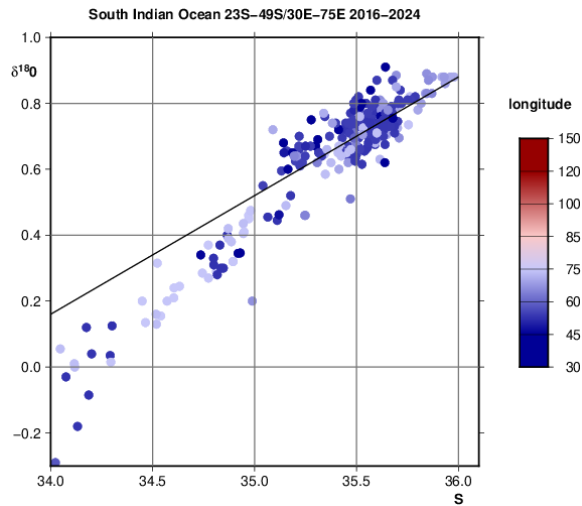
196 the CROCCA-2S data set, albeit not close to west Australia, as well as the area of the
 197 Richardson et al. (2019) data set, south of Australia. The LOCEAN data set also contains
 198 surface data south of Tasmania (in 2017, as well as in 2020 to 2024). All these data
 199 correspond to samples analyzed on a CRDS Picarro L2130 at LOCEAN, and with the
 200 protocols discussed in Reverdin et al. (2022). The bottles in which the samples were
 201 stored were the same for all the samples, and time between collection and analysis
 202 varied, but was mostly on the order of 6 months or less. Thus, this is a homogeneously
 203 produced set of data in for the years 2016-2024, which spatially and temporally
 204 overlaps with the data used in Glaubke et al. (2024) collected south of Australia and in
 205 the southeastern Indian Ocean (Fig. 2).



206
 207 Figure 2: Map of $\delta^{18}\text{O}$ surface data in the LOCEAN archive for 2016-24, north of 60°S . All
 208 these data are associated with S and $\delta^2\text{H}$ data.

209 The LOCEAN data distribution indicates some scatter in the S- $\delta^{18}\text{O}$ distribution in the
 210 southwestern Indian Ocean (Fig. 3a) for S larger than 35. Data above the regression line
 211 on Fig. 3a, established for all data with S between 35 and 36, are present only for S
 212 larger than 35.0, and are found north of 28°S and in the far south-western Indian Ocean,
 213 but with some remnants found all the way to the core of the subtropical gyre near
 214 $75^\circ\text{E}/35^\circ\text{S}$ (Fig. 3b). Data below the regression line contain most of the data south of
 215 28°S and east of 60°E and connect the salinity maximum region with the lower salinity
 216 south of the Subtropical Front and down to the region south of the Polar Front (Fig. 3c).
 217 These subtropical lower values in S- $\delta^{18}\text{O}$ space, which appear in the repeated French
 218 OISO cruises (in 1998-2024) at 50°E , albeit not all the time, dominate east of 60°E .

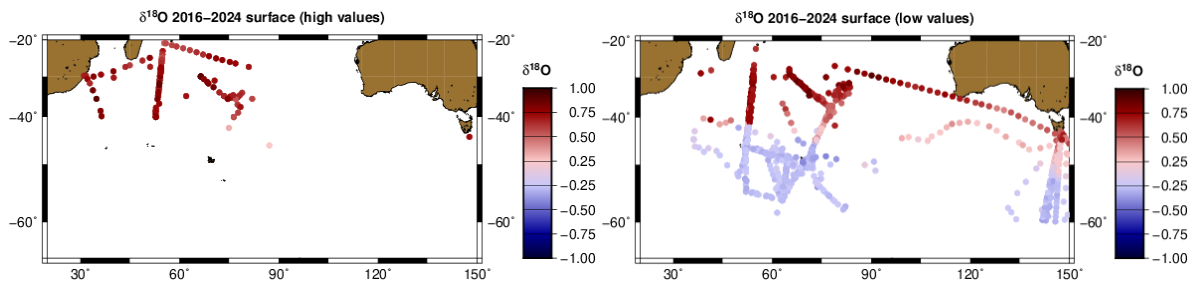
219 a)



220

221 b)

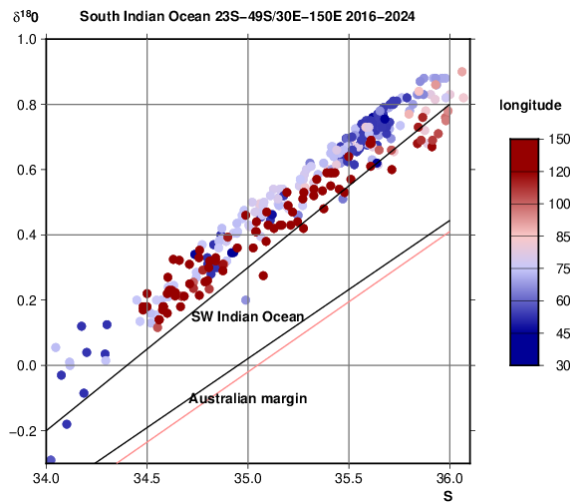
c)



222

223 Figure 3: (a) scatter diagram of (S , $\delta^{18}\text{O}$) 0-30m LOCEAN data within the southwestern
 224 region (30-75°E/23-49°S) coloured as a function of longitude, with the regression line of
 225 the data having a practical salinity between 35 and 36 (black line) overlaid. The spatial
 226 distributions of the LOCEAN data with higher and lower $\delta^{18}\text{O}$ relative to that regression
 227 line in the whole Indian Ocean north of 60°S are shown on panels (b) and (c),
 228 respectively.

229 When focusing on the lower part of the distribution in S - $\delta^{18}\text{O}$ space (Fig. 3c), one
 230 observes a gradual lowering of $\delta^{18}\text{O}$ from west to east for salinities above 35 (Fig. 4) all
 231 the way to 150°E. This lowering is on the order of 0.15 at most, even for the higher
 232 salinities (35.5 or more) for which it is strongest (Fig. 4).



233

234 Figure 4: The 0-30m LOCEAN data below the regression line of Fig. 3a (the ones mapped
 235 in Fig. 3c) in S- $\delta^{18}\text{O}$ space, color-coded as a function of longitude. The two linear
 236 relationships for the 0-100m layer recommended in this region between 23°S and 49°S
 237 by Glaubke et al. (2024) for the south-west Indian Ocean and for the Australian margin
 238 (south of Australia) (we use the original relation $\delta^{18}\text{O} = 0.4231 * S - 14.7876$, instead of
 239 the rounded-up relation reported in the paper; R. H. Glaubke, pers. comm., 2024) are
 240 also plotted (black lines), as well as the earlier linear relationship for the 0-600m layer
 241 along the Australian margin by Richardson et al. (2018) (in pink).

242 Thus, besides some gradual and smaller changes, we do not observe in the LOCEAN
 243 surface dataset a large sudden change in the (S, $\delta^{18}\text{O}$) distribution near 75°E or 85°E
 244 between the southeastern and southwestern Indian Ocean, nor a further strong change
 245 closer to the Australian coastal margin, as suggested by figures 6 and 7 of Glaubke et al.
 246 (2024). Most of the LOCEAN (S, $\delta^{18}\text{O}$) data south of 28°S correspond to the mixing of a
 247 low salinity end-member characteristic of the fresh waters of the Southern Ocean (at $S <$
 248 34) with waters which are imprinted by air-sea exchange of water in a wider range of
 249 values at $S > 36$, as discussed in Glaubke et al (2024). These LOCEAN (S, $\delta^{18}\text{O}$) values are
 250 significantly above the linear relationships proposed by Glaubke et al. (2024). This
 251 positive offset seems to be about 0.15‰ in the southwestern Indian Ocean, but close to
 252 0.50‰ for the Australian coastal margins, although we could not access the individual
 253 data for that latter region. These offsets are much larger than the scatter present in the
 254 LOCEAN data, which is of the order of 0.10 ‰. Furthermore, the LOCEAN data support
 255 the presence of a secondary low salinity end member at $S < 35$ with heavier isotopic

256 composition, contributing to the water mass properties in the far southwestern Indian
257 Ocean as well as for the area sampled between 20°S and 28°S north of the subtropical
258 salinity maximum. This could be a contribution of the Indonesian Through Flow and
259 tropical western Indian Ocean surface waters, as discussed by Kim et al. (2021) and
260 Glaubke et al. (2024). We could not carry out a comparable comparison for $\delta^2\text{H}$ which is
261 not presented in Glaubke et al. (2024), and which exhibits a too large scatter in the
262 CROCCA-2S data set to reach a firm conclusion.

263 3. Discussion

264 In the two comparisons of surface data presented in this note, we find significant
265 differences. Do these differences originate from spatio-temporal variability or from
266 systematic offsets?

267 In the case of the RV Polarstern dataset (Bonne et al., 2019), an error in a specified
268 reference material value was found after the publication, and the adjusted data present
269 only a small, non-significant $\delta^{18}\text{O}$ negative offset, but a significant positive $\delta^2\text{H}$ offset
270 with respect to LOCEAN data. Differences might arise from spatial differences. For
271 example, in the northern hemisphere, values at salinity close to 35 pss mostly originate
272 from the North Sea and English Channel in the Polarstern dataset, thus with more mid-
273 latitude continental influence than for most of the LOCEAN data in the same salinity
274 range which have a contribution of more depleted subpolar and polar freshwater. One
275 expects a larger scatter in the South Atlantic for salinities less than 35, due to
276 intermittent presence of sea ice or iceberg melt, and at higher salinities due to the
277 presence of different water masses originating from the South Atlantic and southeastern
278 Indian Ocean. However, the current data set is not sufficient to estimate it.

279 Furthermore, different seasons were sampled in the two datasets. In the northeastern
280 Atlantic sector, Bonne et al. (2019) surface data east of 30°W were collected in April and
281 November north of 10°S and in November south of 10°S in the southeastern Atlantic.
282 These data do not suggest large seasonal differences in the Northeast Atlantic,
283 concurring with the LOCEAN (S, $\delta^{18}\text{O}$) data in the tropics to mid-latitudes (20 to 50°N),
284 which are tightly distributed along a mean S- $\delta^{18}\text{O}$ relationship, and thus with low
285 seasonal variability (Benetti et al., 2017a; Voelker et al., 2015). The LOCEAN data are

286 not numerous enough in the South-East Atlantic to further evaluate whether the offset is
287 constant throughout the data set, or presents a component related to geographical
288 temporal or spatial variability.

289 To investigate the South Indian Ocean sea water isotopic composition, Glaubke et al.
290 (2024) combined data sets that were processed in different institutes. Potential offsets
291 between those could thus cause apparent spatial variability. In particular, Glaubke et al.
292 (2024) outline large spatial contrasts in the S- $\delta^{18}\text{O}$ relationship across the surface
293 subtropical Indian Ocean and southern Australia that are at least a factor two smaller in
294 the recent version of the LOCEAN database.

295 Seasonal or interannual variability might contribute to the differences shown on Fig. 3,
296 as the data in the southeastern Indian Ocean from Glaubke et al. (2024) were collected
297 in November-December, whereas the data in the LOCEAN database in this region are
298 mostly from February-March. However, at least south of Tasmania, where the LOCEAN
299 data base also contains December data, it does not seem that the seasonal cycle causes
300 differences larger than 0.05 ‰ at the same salinity. A difference due to seasonality
301 would thus be barely identifiable in that case, noting the possible presence of
302 interannual variability and that the long-term accuracy in the analyses in some centers,
303 such as AWI Potsdam and LOCEAN, is 0.05 ‰. Richardson et al. (2018) also commented
304 that south of Australia there was little difference between a southern winter cruise and
305 late summer (March) data. Further west, near 55-70°E, earlier surface data in the OISO
306 surveys, as well as the vertical upper profiles of OISO station data also suggest a rather
307 modest seasonal variability on the order of 0.10‰. Changes could also arise from
308 interannual variability, but the range of interannual variability in the LOCEAN data base
309 is smaller than the difference between the Glaubke et al (2024) curves for the
310 southeastern Indian Ocean and south of Australia and the corresponding LOCEAN data.
311 Thus, a likely cause of the large differences between the South Indian Ocean/Australia
312 margin data combined in the Glaubke et al. (2024) study is the existence of systematic
313 offsets between the data produced in different institutes.

314 4. Conclusions

315 What these two comparisons suggest is that offsets are present between different recent
316 data sets published, which exceed 0.10‰ in $\delta^{18}\text{O}$ and 0.50‰ in $\delta^2\text{H}$, thus larger than the
317 target long-term accuracy of analyses in individual isotopic laboratories. Moreover,
318 errors in reference material values are always possible and require post-analysis
319 intercomparisons, such as the one that led to the correction of the RV Polarstern Bonne
320 et al. (2019) data set. Furthermore, one contribution to a systematic difference between
321 the LOCEAN data set and data from other institutes is that the LOCEAN data are
322 reported in ‘freshwater’ concentration scale (Benetti et al., 2017b). The use of this
323 concentration scale corrects possible effects of salt in the water activity measured by
324 IRMS with CO_2 -equilibration and the effect of salt accumulation during evaporation in
325 laser spectroscopy, which both can lead to fractionation, possibly of similar magnitude
326 (Walker et al., 2016). Different comparisons based on duplicates collected during cruises
327 suggest that this is a main cause of difference between LOCEAN data and other data sets
328 (LOCEAN $\delta^{18}\text{O}$ data been more positive). Poor conservation of the samples during
329 storage, analytical protocols, or uncertainties in the specified values of reference
330 material are other sources of differences between data produced in different institutes.

331 The methods for intercomparing and detecting systematic offsets between different data
332 sets are not numerous. On one hand, one could compare values obtained in specific
333 water masses, for which we expect little variability of the water isotopic composition.
334 This is often used, but such data are not always available, and the resulting uncertainties
335 are difficult to assess, although data sets with deep data in the Southern Ocean might be
336 used to test this approach. One could also develop a method based on the systematic
337 comparison of nearby data, as is suggested in Fig. 1 when comparing the S-water
338 isotopes surface distribution in the North and South Atlantic in the LOCEAN and the RV
339 Polarstern (Bonne et al., 2019) data sets. This could be further improved, but requires
340 that there are enough overlapping data within regions of relatively homogeneous
341 signals.

342
343 As the data density is not always sufficient, these approaches may fail. Thus, an
344 important complementary approach is to actively share well-preserved water samples,
345 distributed quickly, and dedicated to specific intercomparison of data produced in the
346 different laboratories, building on previous efforts for $\delta^{13}\text{C}$ -DIC (Cheng et al., 2019).

347 This, together with establishing well-accepted guidelines for data production and quality
348 control, and enhancing scientific exchange between the different institutes needs to be
349 actively pursued, in order to reduce the errors when merging different datasets and
350 increase the potential use of the water isotope data as EOVS/ECCVs. This approach is
351 recommended by the recently established working group MASIS (Towards best practices
352 for Masuring and Archiving Stable Isotopes in S seawater) of the Scientific Committee of
353 Oceanic Research (SCOR). Without such direct intercomparison of samples, the
354 usefulness of the isotopic data for different oceanographic and climate studies is
355 strongly reduced, for example resulting in large uncertainties when establishing
356 different S- $\delta^{18}\text{O}$ (or S- $\delta^2\text{H}$) relationships to validate studies of proxies to support paleo-
357 climate reconstructions.

358

359 Data availability

360 The LOCEAN data are available at <https://www.seanoe.org/data/00600/71186/>.
361 The isotopic data of the Bonne et al. (2019) are available as indicated in the paper, with
362 here S added from the PANGAEA archive, as described in the text. The Glaubke et al.
363 (2024) data are available as described in the paper. However, among the data used in
364 this paper, we could not access the data from the Richardson et al. (2019) paper.

365

366 Author contribution: GR initiated the study and prepared the manuscript with
367 contributions from all coauthors. AV initiated the intercomparison effort, and AV, CW,
368 and HM contributed to editing the paper. HM was also responsible from producing the
369 data in the Bonne et al. (2019) paper.

370

371 Competing interests: The authors declare that they have no conflict of interest.

372

373 Acknowledgments

374 The LOCEAN isotopic laboratory is supported by OSU Ecce Terra of Sorbonne Université.
375 We are thankful to Catherine Pierre and Jérôme Demange who have set and help run the
376 facility, and for Aïcha Naamar, Marion Benetti and Camille Akhoudas to have measured
377 some of the water samples. We are grateful for support by INSU, Nicolas Metzl and Claire
378 Lo Monaco for samples during the OISO cruises on RV MD2, by IPEV during the SOCISSE
379 program on RV Astrolabe, with on board support by Patrice Bretel and Rémi Foletto, and

380 by IPSL for supporting the LOCEAN data base and intercomparisons. Antje Voelker
381 thanks Joanna Waniek (IOW, Germany) for collecting the NE Atlantic water samples and
382 Robert van Geldern (GeoZentrum Nordbayern, Germany) for analyzing them. She, also,
383 acknowledges financial support by Fundação para a Ciência e a Tecnologia (FCT) through
384 projects Centro de Ciências do Mar do Algarve (CCMAR) basic funding
385 UIDB/04326/2020 (<https://doi.org/10.54499/UIDB/04326/2020>) and programmatic
386 funding UIDP/04326/2020 (<https://doi.org/10.54499/UIDP/04326/2020>) and the
387 CIMAR associated laboratory funding LA/P/0101/2020
388 (<https://doi.org/10.54499/LA/P/0101/2020>). The RV Polarstern data set was funded
389 by the AWI Strategy Fund Project ISOARC. Comments by Alexander Haumann (AWI) and
390 by two anonymous reviewers were very helpful.

391

392 References

393 Aoki, S., Kobayashi, R., Rintoul, S. R., et al. : Changes in water properties and flow regime
394 on the continental shelf off the Adélie/George V Land coast, East Antarctica, after glacier
395 tongue calving, *J. Geophys. Res.: Oceans*, 122, 6277-6294, 2017.

396 Akhoudas, C. H., Sallée, J.-B., Haumann, F. A., Meredith, M. P., Garabato, A. N., Reverdin,
397 G., Jullion, L., Aloisi, G., Benetti, M., Leng, M. J., and Arrowsmith, C.: Ventilation of the
398 abyss in the Atlantic sector of the Southern Ocean, *Nature scientific reports*, **11**, 16733,
399 <https://doi.org/10.1038/s41598-021-95949-w>, 2020, 2021.

400 Atwood, A. R., Moore, A.L., Long, S., Pauly, R., DeLong, K., Wagner, A., and Hargreaves, J.A.:
401 The CoralHydro2k Seawater $\delta^{18}\text{O}$ Database, *Past Global Changes Magazine* 32,59, doi:
402 10.22498/pages.32.1.59, 2024.

403 Benetti, M., Reverdin, G., Aloisi, G., and Sveinbjörnsdóttir, A.: Stable isotopes in surface
404 waters of the Atlantic Ocean: indicators of ocean-atmosphere water fluxes and oceanic
405 mixing processes. *J. Geophys. Res. Oceans*, doi:10.1002/2017JC012712, 2017a.

406 Benetti, M., Sveinbjörnsdóttir, A. E., Ólafsdóttir, R., Leng, M. J., Arrowsmith, C., Debondt,
407 K., Fripiat, F., and Aloisi, G.: Inter-comparison of salt effect correction for $\delta^{18}\text{O}$ and $\delta^2\text{H}$
408 measurements in seawater by CRDS and IRMS using the gas-H₂O equilibration method,
409 *Marine chemistry*, doi:10.1016/j.marchem.2017.05.010, 2017b.

410 Biddle, L. C., Loose, B., and Heywood, K. J.: Upper ocean distribution of glacial meltwater
411 in the Amundsen Sea, Antarctica. *J. Geophys. Res. Oceans*, 10.1029/2019JC015133. et al.,
412 2019:

- 413 Bonne, J.-L., Behrens, M. Meyer, H., Kipfstuhl, S., Rabe, B., Schönicke, L., Steen-Larsen, H.
414 C., Werner, M.: Resolving the controls of water vapour isotopes in the Atlantic sector.
415 Nature Comm. 10, 1632, doi: 10.1038/s41467-019-09242-6, 2017.
- 416 Boutin, J., Chao, Y., Asher, W. E., Delcroix, T., Drucker, D., et al. : Satellite and In Situ
417 Salinity: Understanding Near-Surface Stratification and Subfootprint Variability. Bull. of
418 the Amer. Meteor. Soc., 97 (8), pp.1391-1407. 10.1175/BAMS-D-15-00032.1, 2016.
- 419 Brady, E., Stevenson, S., Bailey, D., Liu, Z., Noone, D., Nusbaumer, J., Otto-Bliesner, B. L.,
420 Tabor, C., Thomas, R., Wong, T., Zhang, J., Zhu, J.:The connected isotopic water cycle in
421 the Community Earth System Model Version 1, J. Adv. Model. Earth Syst., 11, 8,
422 <https://doi.org/10.1029/2019MS001663>, 2019.
- 423 Cauquoin, A., Werner, M., Lohmann, G.: Water isotopes – climate relationships for the
424 mid-holocene and preindustrial period simulated with an isotope-enabled version of
425 MPI-ESM, Clim. Past 15, 1913-1937, <https://doi.org/10.5194/cp-15-1913-2019>, 2019.
- 426 Cheng, L., Normandeau, C., Bowden, R., Doucett, R., Gallagher, B., Gillikin, D. P.,
427 Kumamoto, Y., McKay, J. L., Middlestead, P., Ninnemann, U., Nothaft, D., Dubinina, E. O.,
428 Quay, P., Reverdin, G., Shirai, K., Mørkved, P. T., Theiling, B.P., van Geldern, R., and
429 Wallace, D. W. R.: An international intercomparison of stable carbon isotope
430 composition measurements of dissolved inorganic carbon in seawater, Limnology and
431 Oceanography: Methods 17, 200-209, <https://doi.org/10.1002/lom3.10300>, 2019.
- 432 Glaubke, R. H., Wagner, A., and Sikes, E. L.: Characterizing the stable oxygen isotopic
433 composition of the southeast Indian Ocean, Marine Chemistry, 262,
434 <https://doi.org/10.1016/j.marchem.2024.104397>, 2024.
- 435 Haumann, F. A. et al. : [Data set], Zenodo, doi:10.5281/zenodo.1494915, 2019.
- 436 Hennig, A., Mucciarone, D. A., Jacobs, S. S., Mortlock, R. A., and Dunbar, R. B.:Meteoric
437 water and glacial meltwater in the southeastern Amundsen Sea: a time series from 1994
438 to 2020, The cryosphere, 18, 791-818, <https://doi.org/10.519/tc-18-791-2024>, 2024.
- 439 Hilaire-Marcel, C., Kim, S. T., Landais, A., Ghosh, P., Assonov, S., Lécuyer, C., Blanchard, M.,
440 Meijer, H. A., and Steen-Larsen, H. C.: A stable isotope toolbox for water and inorganic
441 carbon cycle studies, Nature Reviews Earth & Environment 2 (10), 699-719, 2021.

- 442 Kim, Y., Rho, T., and Kang, D.-J.: Oxygen isotope composition of seawater and salinity in
443 the western Indian Ocean: Implications for water mass mixing, *Mar. Chem.* 237, 104035,
444 <https://doi.org/10.1016/j.marchem.2021.104035>, 2021.
- 445 Konecky, B. L. et al.: The Iso2k database: a global compilation of paleo- $\delta^{18}\text{O}$ and $\delta^2\text{H}$
446 records to aid understanding of Common Era climate, *Earth Syst. Sci. Data*, 12, 2261–
447 2288, <https://doi.org/10.5194/essd-12-2261-2020>, 2020.
- 448 Kumar, P. K., Singh, A., and Ramesh, R.: Convective mixing and transport of the Bay of
449 Bengal water stir the $\delta^{18}\text{O}$ -salinity relation in the Arabian Sea., *J. Mar. Sys.* 238, 103842,
450 <https://doi.org/10.1016/j.jmarsys.2022.103842>, 2023.
- 451 LeGrande, A. N. and Schmidt, G. A.: Global gridded data set of the oxygen isotopic
452 composition in seawater, *Geophys. Res. Lett.* 33,
453 <https://doi.org/10.1029/2006gl026011>, 2006.
- 454 Oppo, D. W., Schmidt, G. A., and LeGrande, A. N.: Seawater isotope constraints on tropical
455 hydrology during the Holocene, *Geophys. Res. Lett.* 34, L13701,
456 <https://doi.org/10.1029/2007GL030017>, 2007.
- 457 Randall-Goodwin, E., Meredith, M. P., Jenkins, A., Yager, P. L., Sherrell, R. M., Abrahamsen,
458 E. P., Guerrero, R., Yuan, X., Mortlock, R. A., Gavanoan, K., Alderkamp, A.-C., Ducklow, H.,
459 Robertson, R., and Stammerjohn, S. E.: Freshwater distributions and water mass
460 structure in the Amundsen Sea polynya region, Antarctica. *Elementa: Science of the*
461 *Anthropocene*, 3: 000065, <https://doi.org/10.12952/journal.elementa.000065>, 2015.
462 et al., 2015.
- 463 Reverdin, G., et al.: The CISE-LOCEAN sea water isotopic database (1998-2021), *Earth*
464 *sci. sys. data*, <https://doi.org/10.5194/essd-2022-34>, 2022.
- 465 Richardson, L. E., Middleton, J. F., Kyser, T. K., James, N. P., and Opdyke, B. N.: Shallow
466 water masses and their connectivity along the southern Australian continental margin,
467 *Deep Sea Res. I, Oceanogr. Res. Pap.* 152, 103083,
468 <http://doi.Org/10.1016/j.dsr.2019.103083>, 2019.
- 469 Schmidt, G. A., LeGrande, A. N., and Hoffmann, G.: Water isotope expressions of intrinsic
470 and forced variability in a coupled ocean-atmosphere model, *J. Geophys. Res.* 112,
471 D10103, <https://doi.org/10.1029/2006jd007781>, 2007.
- 472 Voelker, A., Colman, A., Olack, G., Waniek, J. J., and Hodell, D.: Oxygen and hydrogen
473 isotope signatures of Northeast Atlantic water masses, *Deep-Sea Res. II*, 116, 89-106.
474 <https://doi.org/10.1016/j.dsr2.2014.11.006>, 2015.

- 475 Voelker, A. H.: Seawater oxygen and hydrogen stable isotope data from the upper water
476 column in the North Atlantic Ocean (unpublished data). Interdisciplinary Earth Data
477 Alliance (IEDA), <https://doi.org/10.26022/IEDA/112743>, 2023.
- 478 Walker, S. A., Azetsu-Scott, K., Normandeau, C., Kelly, D. E., Friedrich, R., Newton, R.,
479 Schlosser, P., McKay, J. L. Abdi, W., Kerrigan, E., Craig, S. E., and Wallace, D. W. R.: Oxygen
480 isotope measurement of seawater ($\text{H}_2^{18}\text{O}/\text{H}_2^{16}\text{O}$). A comparison of cavity ring-down
481 spectroscopy (CRDS) and isotope ratio mass spectrometry (IRMS), *Limnol. and*
482 *Oceanography: Methods*, 14, 31-38, <https://doi.org/10.1002/lom3.10067>, 2016.